Article

HAADF STEM and Ab Initio Calculations Investigation of Anatase TiO_2/$LaAlO_3$ Heterointerface

Mahabul Islam [1] , **Piu Rajak** [1] , **Daniel Knez** [2] , **Sandeep Kumar Chaluvadi** [1] , **Pasquale Orgiani** [1] , **Giorgio Rossi** [1,3] , **Goran Dražić** [4] **and Regina Ciancio** [1,*]

1   Istituto Officina dei Materiali-CNR, Area Science Park, S.S.14, Km 163.5, 34149 Trieste, Italy; islam@iom.cnr.it (M.I.); rajak@iom.cnr.it (P.R.); chaluvadi@iom.cnr.it (S.K.C.); orgiani@iom.cnr.it (P.O.); giorgio.rossi2@unimi.it (G.R.)
2   Institute for Electron Microscopy and Nanoanalysis, Graz University of Technology, Steyrergasse 17, 8010 Graz, Austria; daniel.knez@felmi-zfe.at
3   Dipartimento di Fisica, Università degli Studi di Milano, Via Celoria 16, 20133 Milano, Italy
4   Department of Materials Chemistry, National Institute of Chemistry, 1001 Ljubljana, Slovenia; goran.drazic@gmail.com
*   Correspondence: ciancio@iom.cnr.it

Abstract: The understanding of the origin of a two-dimensional electron gas (2DEG) at the surface of anatase TiO_2 remains a challenging issue. In particular, in TiO_2 ultra-thin films, it is extremely difficult to distinguish intrinsic effects, due to the physics of the TiO_2, from extrinsic effects, such as those arising from structural defects, dislocations, and the presence of competing phases at the film/substrate interface. It is, therefore, mandatory to unambiguously ascertain the structure of the TiO_2/substrate interface. In this work, by combining high angle annular dark-field scanning transmission electron microscopy (HAADF-STEM), density functional theory calculations, and multislice image simulations, we have investigated the nature of strainless anatase TiO_2 thin films grown on $LaAlO_3$ substrate. In particular, the presence of oxygen vacancies in anatase TiO_2 has been proved to stabilize the formation of an extra alloy layer, Ti_2AlO_4, by means of interface rearrangement. Our results, therefore, elucidate why the growth of anatase TiO_2 directly on $LaAlO_3$ substrate has required the deposition of a TiO_x extra-layer to have a 2DEG established, thus confirming the absence of a critical thickness for the TiO_2 to stabilize a 2DEG at its surface. These findings provide fundamental insights on the underlying formation mechanism of the 2DEG in TiO_2/LAO hetero-interfaces to engineer the 2DEG formation in anatase TiO_2 for tailored applications.

Keywords: anatase TiO_2; 2DEG; oxygen vacancies; heterointerfaces; aberration-corrected scanning transmission electron microscopy; DFT calculations; image simulations

1. Introduction

Over the last decades, novel phenomena and functionalities at artificial heterointerfaces have been attracting extensive interest in both materials science and fundamental condensed matter physics. Thanks to the considerable advancements in thin-film growth, the electrostatic boundary conditions at oxide surfaces and interfaces can be used to epitaxially design artificial heterointerfaces with atomic precision, to form new electronic phases, or novel low-dimensional states usually inaccessible in the bulk oxides. Two-dimensional free-electron gases (2DEG) [1,2] ferromagnetism between two non-magnetic materials [3,4] and interface electronic reconstruction [5] are prominent examples of exotic phenomena emerging at heterointerfaces between oxide layers with properties differing from either constituent, thus suggesting new possible platforms for a future generation of technological applications [6]. In this regard, understanding the physical mechanisms responsible for the formation of a 2DEG at the surface of insulating oxides or at their interface remains one of the most challenging issues. For instance, in the case of $SrTiO_3$-based interfaces,

many reports have, indeed, pointed towards the building of an internal electrical potential as a mandatory condition to drive the formation of the 2DEG. Such a scenario appears to be confirmed by the existence of a threshold thickness of the oxide layers as the onset of the highly conductive state [7,8]. However, alternatively, extrinsic mechanisms attributed to local structural imperfections (mainly oxygen vacancies) have been suggested to be responsible for the arising of the 2DEG, with no need of a critical thickness [9–11], thus still leaving the debate open. This is also the case of anatase TiO_2. Some reports point to a three-dimensional character of the TiO_2 surface [12], while others support a two-dimensional nature [13,14] or the coexistence of both 2D and 3D characters [15], similar to other oxide systems. Having access to a very high-quality single-unit-cell (and sub-unit-cell) layer of a given material is the only way to provide conclusive evidences on the dimensionality issue.

In this framework, very recently, some of the authors have demonstrated that no critical thickness is required to stabilize the 2DEG at the anatase TiO_2 surface and implying its purely 2D nature after optimization of the synthesis process, which demands the use of a functional buffer layer of $LaNiO_3$ [16]. However, the growth of anatase TiO_2 directly on $LaAlO_3$ substrate has required the deposition of a TiO_x extra-layer to have a 2DEG established, thus questioning the validity of the scenario in which no critical thickness is required [16].

In the present work, we provide an in-depth investigation of the film/substrate interface of anatase TiO_2 thin films grown on LAO (001) substrates by pulsed laser deposition (PLD). By resorting to spherical aberration-corrected scanning transmission electron microscopy (STEM) high angle annular dark field imaging (HAADF) complemented by multi-slice simulations based on relaxed structures obtained from ab initio calculations, we determined the intrinsic structure of the TiO_2/LAO interface. With our approach, we validated a new model which strongly relies on the fact that the intrinsic reduced nature of TiO_2 anatase films, demonstrated in our previous work [17], is prone to stabilize a Ti_2AlO_4 alloy in the very initial layers of the film, as a result of the competition between the structural parameters of the two interfacing oxides. To the best of our knowledge, no previous report considered the presence of an oxygen-deficient anatase structure to describe the formation of a new phase near the film/substrate interface. By means of density functional theory (DFT) calculations on oxygen deficient structures, we relate the evolution of the interfacial structure to the ionic relaxation at the interface. The identification of an alien chemical/structural phase at the very initial stage of anatase TiO_2 growth, though confined in a single-layer-thick region at the film/substrate interface, further confirms the truly 2D nature of the 2DEG in anatase TiO_2 and the absence of a critical thickness as the origin of its occurrence.

2. Materials and Methods

2.1. Thin-Film Growth

Anatase TiO_2 thin film was grown by pulsed laser deposition (PLD) technique at the APE-IOM laboratory (NFFA facility, Trieste, Italy) [18–22]. TiO_2 single crystal of rutile phase was ablated using a KrF excimer pulsed laser with a repetition rate of 3 Hz and an energy density of roughly 2 J/cm^2. The growth temperature of the substrate was kept at 700 °C and the oxygen partial pressure was maintained at 10^{-4} mbar. Annealed samples were maintained at the growth temperature for 10 min in ultra-high vacuum (~10^{-7} mbar) [23].

2.2. HRTEM and HAADF STEM Experiments

Cross-sectional TEM samples were prepared by conventional polishing technique followed by dimpling and ion milling performed by a precision ion polishing system (PIPS). The JEOL 2010 UHR field emission gun microscope was used to acquire high-resolution TEM (HRTEM) images at 200 kV with a measured spherical aberration coefficient C_s of 0.47 ± 0.01. The sample was tilted to the [010] zone axis to align the film growth direction perpendicular to the electron beam direction.

Aberration corrected Scanning TEM (STEM) analyses were performed on a cold field emission type C_s probe corrected ARM-200 CF, JEOL Ltd. operating at 200 kV with a convergence angle of 24 mrad. The inner and outer detection angles of the HAADF detector were 68 and 185 mrad, respectively. The sample was oriented to the [010] axis of the thin film and the fast-scanning direction was oriented perpendicular to the interface.

2.3. DFT Calculations

To benchmark the pseudopotentials, first the bulk properties, such as equilibrium lattice parameters and electronic bandgaps, were calculated within accepted accuracy. With the optimized lattice parameters, surface-cells were built along the required directions for both the phases of the hetero-structures. Two types of terminations were considered for LAO substrate, e.g., AlO_2 and LaO terminations for the [001] LAO substrate. The interface model was relaxed using first-principle approaches within the scope of DFT in order to confirm experimental observations theoretically. The DFT calculations have been performed using the Quantum Espresso [24] code using the Perdew–Burke–Ernzerhof (PBE) exchange-correlation functional [25] as incorporated in the ultrasoft pseudopotentials. The valence electron configuration for the La, Ti, Al, and O atoms were $5s^05p^15d^26s^06p^1$, $3s^03p^13d^2\,4s^0$, $3s^03p^1$, and $2s^02p^1$, respectively. For the optimization of the heterostructure models, the plane-wave wavefunctions cutoff and the charge-density cutoff were set as 35 Ry and 210 Ry, respectively. The ionic positions and the lattice parameters were relaxed using the BFGS (Broyden–Fletcher–Goldfarb–Shanno) algorithm until the forces on each atom were converged below 1 m eV/Å (1.6×10^{-12} N) for the bulk calculations. All atoms of the slabs were fully relaxed until the force on each atom reached less than 0.01 eV/Å (1.6×10^{-11} N).

2.4. STEM-HAADF Image Simulation

Multislice calculations were used to simulate STEM-HAADF images from the DFT relaxed structures to match the experimental observation. The QSTEM [26] software was used to perform frozen phonon calculations with the same parameters as of the experiment: 200 kV acceleration voltage, 24 mrad convergence angle, 0.005 mm C_s, 0.8 eV energy-spread (dE), and −4.3 nm defocus with a total of 15 phonon configurations. The slice thickness of the model with 19 nm thickness along the electron beam direction was chosen 1.9 Å. Like in the experiment, the interface structure was oriented along viewing direction [010].

3. Results and Discussions

In Figure 1a, a representative cross-sectional bright-field TEM image of the TiO_2/LAO heterostructure taken in the [010] zone axis of the substrate is shown. The TiO_2 film has a good crystalline quality and shows the typical modulated structure of the reduced anatase structure reported in earlier works [17,27,28]. The TiO_2/LAO interfaces appear sharp and atomically flat. The corresponding selected area electron diffraction (SAED) pattern shown in Figure 1b indicates very good crystalline matching between the TiO_2 film and the LAO substrate with a TiO_2 (001)∥ LAO (001) epitaxial relationship.

To gain more insight into the atomic structure of the TiO_2/LAO interface, we performed advanced STEM-HAADF experiments with a C_s-corrected microscope, since HAADF provides the atomic sites of heavy elements, which enable us to visualize oxide interfaces [29–31]. A representative STEM-HAADF image of the TiO_2/LAO heterostructure is shown in Figure 2a. The predominant signal in the film comes from the typical dumbbell structure of TiO_2 anatase, while the signal of the substrate is dominated by the heaviest La ions (labels are superimposed to the image for ease of visualization). In Figure 2b, an enlarged view of the interface region is provided and marked with a cyan-colored dashed box. The atomic stacking in the vicinity of the interface is strikingly different from both the substrate and the film. This can be better appreciated from the magnified image of Figure 2b, where extra atoms (marked with white arrows) can be identified with a relative distance of half of the unit cell of anatase along the [100] direction.
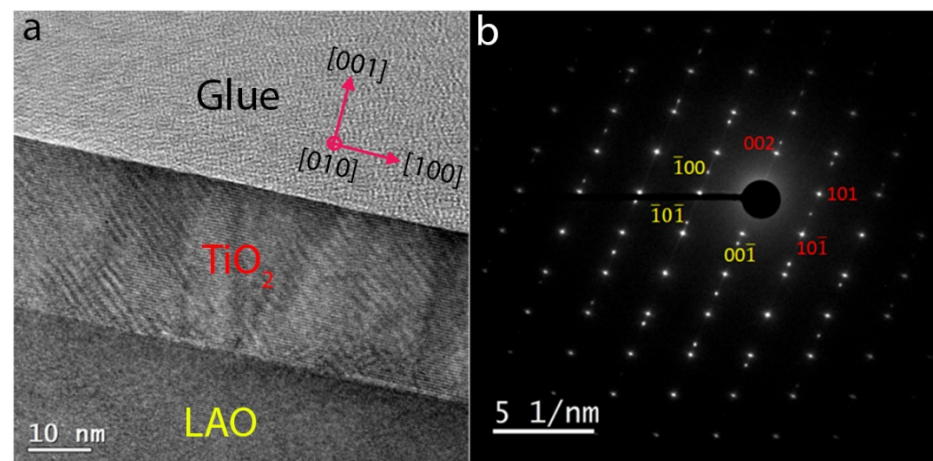
Figure 1. (**a**) Cross-sectional TEM image of the TiO_2/LAO interface. (**b**) The SAED patterns at the TiO_2/LAO interface correspond to [010] zone-axis.
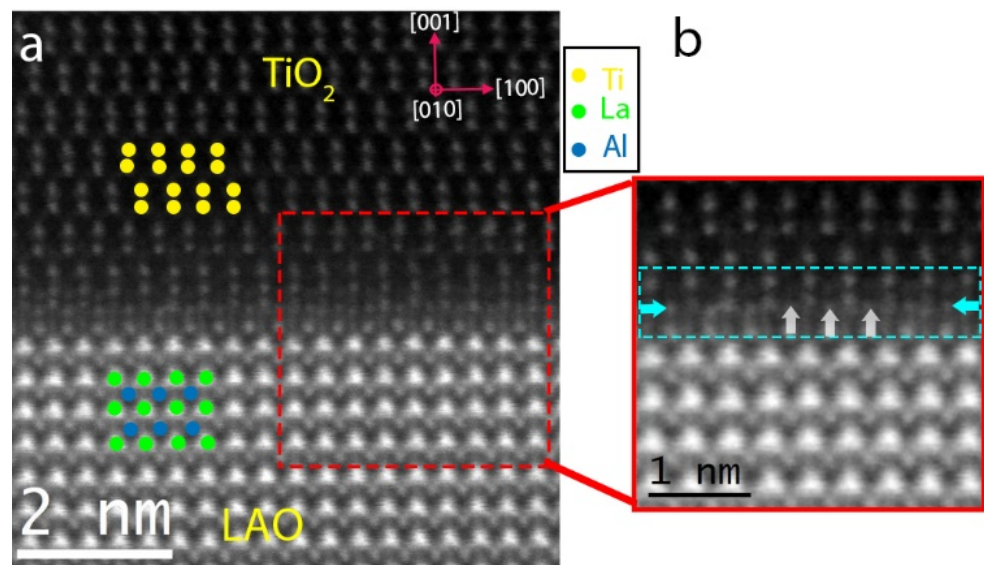
**Figure 2.** (**a**) A cross-sectional STEM-HAADF image of the interface TiO_2/$LaAlO_3$ viewed along the [010] direction. Green, blue, and yellow solid circles indicate La, Al, and Ti columns, respectively. (**b**) The interface is marked by a dashed cyan-colored box pointed with cyan arrows. The white arrows point at the extra atoms at the first interfacial layer.

According to the general strategy reported in the literature [32], we evaluated the possibility of a TiO_2 on AlO_2- and LaO-terminated LAO substrate to reproduce the interfacial structure of our experimental data. In both cases, we cannot reproduce the presence of extra spots that are clearly evident in our experimental data, as well as in the reported literature [33]. We, therefore, evaluated the possibility of other structural phases based on the element present at the film/substrate interface and spacings compatible with the experimental data. Among these, a good candidate is represented by Ti_2AlO_4, which has lattice parameters of a = 5.66 Å, b = 6.08 Å, and c = 8.13 Å for the conventional unit-cell belonging to the 'Imma' (74) Hermann Mauguin space-group [34]. Moreover, since the 2DEG is known to occur in O-deficient anatase [16], we performed DFT calculations starting from an O-deficient anatase structure and considering two different possible interfacial terminations of the LAO substrate, namely AlO_2 and LaO. All the parameters used for the calculation are provided in the materials and methods section.

At first, to identify the interfacial termination of LAO substrate, the bulk unit cells of LAO and Ti_2AlO_4 were relaxed using DFT as implemented in the Quantum Espresso

software suite [24]. With the optimized coordinates, surface slabs were built along [001] and [110] for LAO and Ti_2AlO_4, respectively. The lattice parameters for the (2 × 2) LAO [001] surface slab were optimized to be a = b = 7.55 Å and those for (1 × 1) Ti_2AlO_4 (110) were optimized to be a = 8.13 Å and b = 8.31 Å. For building the surface slab, surface energy convergence was tested against the surface slab thickness to ensure bulk-like behavior for the substrate. To mimic the atomic stacking of the experimental image of Figure 2b, at first, a two-layer surface slabs were built by seven layers (2 × 2) LAO (001) and five layers of (1 × 1) Ti_2AlO_4 (110) with two types of LAO surface terminations: AlO_2 and LaO termination. For building this heterostructure, (1 × 1) Ti_2AlO_4 (110) was strained to twice the substrate lattice parameter of a = b = 7.55 Å. In Figure 3, two types of substrate termination models for the unrelaxed configurations are shown for Ti_2AlO_4 (110) on LAO (001). Among these two models, the most favorable termination is found to be AlO_2 by calculating the interface formation energy [32], although the formation energies of the two types of terminations are almost identical. By visual cues from the HAADF contrast of Figure 2b, it was confirmed that the termination is indeed AlO_2 termination.
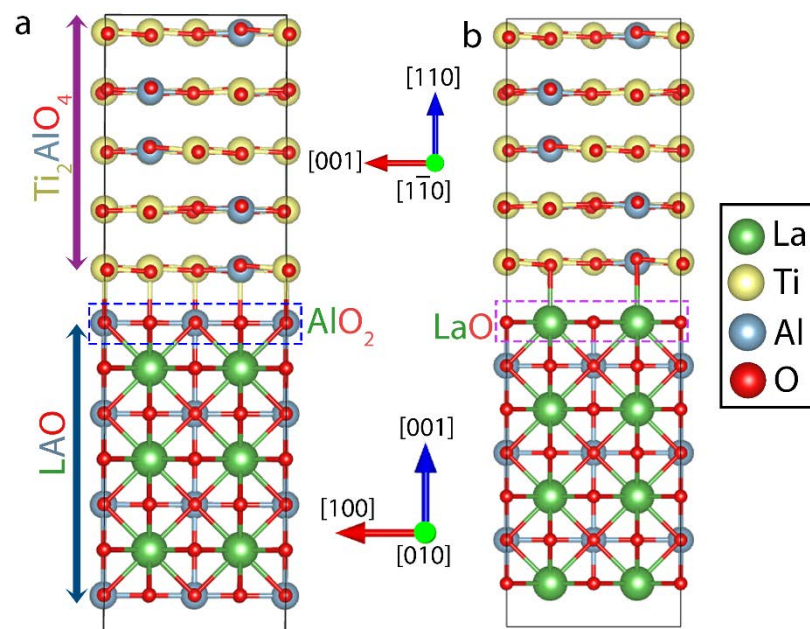
Figure 3. (**a**) A schematic of the unrelaxed AlO_2 terminated-$LaAlO_3$ (001)/Ti_2AlO_4 (110) is shown; (**b**) schematic of the unrelaxed LaO terminated-$LaAlO_3$ (001)/Ti_2AlO_4 (110). The legends for the atom types are given in the inset.

Based on these optimized bilayer models, a tri-layer supercell was then created to match experimental observation (Figure 4) by stitching pure anatase (without oxygen vacancies) TiO_2 and O-deficient anatase TiO_2 to one monolayer of (1 × 1) Ti_2AlO_4 (110) on AlO_2-terminated LAO (stackings are described from the top of Figure 4). The model configurations were built along the [001] direction with seven atomic layers of LAO, one monolayer of Ti_2AlO_4, and nine layers of anatase TiO_2. These layer thicknesses were sufficient to represent the bulklike properties. The DFT-relaxed interfaces of Ti_2AlO_4/pure-TiO_2 and Ti_2AlO_4/O-deficient-TiO_2 are shown in Figure 4a,b, respectively. The red arrows in Figure 4a,b show the force vectors due to DFT relaxation. The positions of random oxygen vacancies within the O-deficient TiO_2 structure are shown with magenta arrows in Figure 4c. By comparing Figure 4a,b, it is observed that the creation of the O-vacancy affects the interface rearrangement differently. The different directions of force vectors acting at the alloy layer give rise to different equilibrium distances in the interface region. The equilibrium interface layer spacings between extra-layer Ti_2AlO_4 and TiO_2 are 3.1 Å and 2.1 Å for the configurations in Figure 4a,b, respectively. To check the structural stability of such a heterostructure, we further calculated the interface adhesion energy [32], which

confirms that the heterostructure model of Figure 4b is dynamically more stable than the pure anatase model (Figure 4a). In addition, the force acting on atoms (red arrows) presented in Figure 4b shows that the region near the interface (marked with the magenta-colored dashed box) favors bonding with O-deficient TiO$_2$.
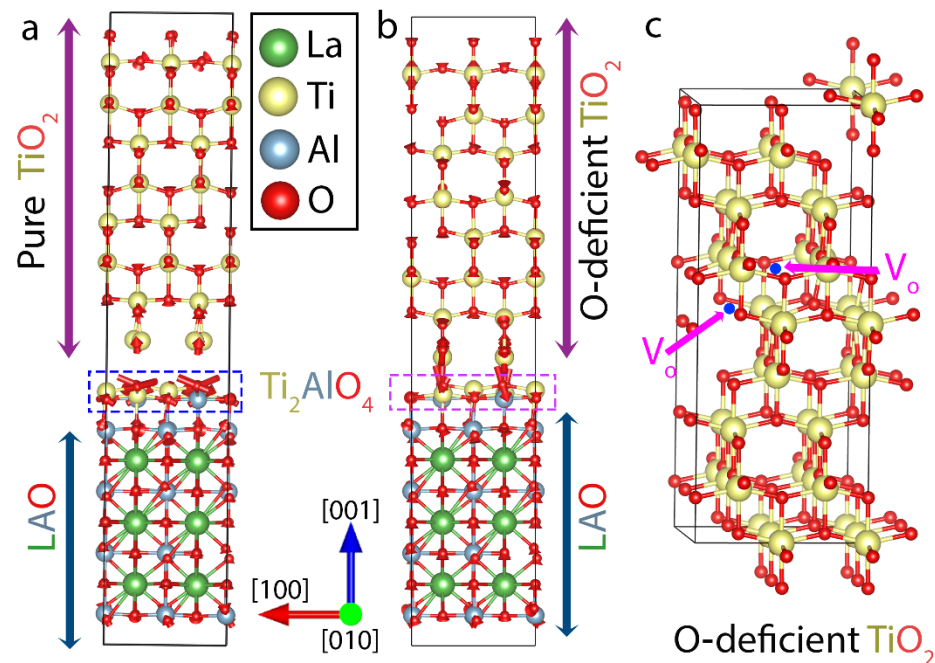
Figure 4. Relaxed structures of the (**a**) AlO$_2$-terminated LaAlO$_3$/Ti$_2$AlO$_4$/pure-TiO$_2$ and (**b**) AlO$_2$-terminated LaAlO$_3$/Ti$_2$AlO$_4$/O-deficient-TiO$_2$ is shown. The red arrows in (**a**,**b**) show the force vectors due to DFT relaxation. (**c**) Schematic of the O-deficient-TiO$_2$ structures, where the sites of V$_O$ (blue circles) are shown with magenta arrows.

In order to compare the interface models with the experimental evidences, STEM-HAADF simulations were performed for both these (Figure 4) geometry-optimized structures using QSTEM software [26]. The optimized coordinates were repeated along the electron-beam direction to create a model thickness of 19 nm, consistent with previously calculated model thickness [17]. The simulated STEM-HAADF images of AlO$_2$-terminated LaAlO$_3$/Ti$_2$AlO$_4$/pure-TiO$_2$ and LaAlO$_3$/Ti$_2$AlO$_4$/O-deficient-TiO$_2$ are shown in Figure 5a,b, respectively. The interfacial extra layer, Ti$_2$AlO$_4$ is marked with arrows in Figure 5. The measured spacings between the extra Ti$_2$AlO$_4$ layer and TiO$_2$ film (marked with cyan-colored dotted box in Figure 5a–c) are 3.1 Å (Figure 5d), 2.2 Å (Figure 5e) and 2.3 Å (Figure 5f), for Figure 5a–c, respectively. This indicates that the LaAlO$_3$/Ti$_2$AlO$_4$/O-deficient-TiO$_2$ model is in a very good agreement with the experimental image presented in Figure 5c. Our results provide strong evidence that the oxygen vacancies in TiO$_2$ play a crucial role in stabilizing the alloy Ti$_2$AlO$_4$ layer at the interface between film and substrate.
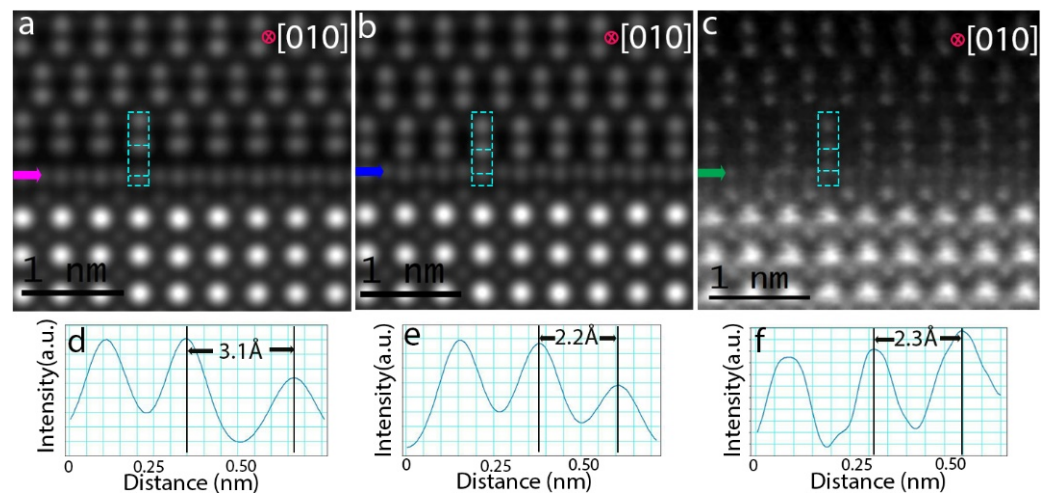
Figure 5. Simulated STEM-HAADF image along the [010] zone axis of (**a**) AlO_2-terminated $LaAlO_3/Ti_2AlO_4/$pure-TiO_2 and (**b**) AlO_2-terminated $LaAlO_3/Ti_2AlO_4/$O-deficient-TiO_2 is shown. (**c**) An experimental STEM-HAADF image along the [010] zone axis of the heterostructure is shown; the arrows in (**a**–**c**) denote the position of the interface alloy layer. (**d**–**f**) Corresponding line profiles taken from the dashed rectangular regions are shown.

4. Conclusions

In summary, we have explored the interface structure of a $TiO_2/$LAO heterointerface using combined STEM-HAADF imaging, multislice image simulations, and DFT calculations. The atomically resolved STEM-HAADF image acquired with aberration-corrected TEM provides clear evidence of the presence of the extra layer at the very initial stage of TiO_2 growth on the LAO substrate. Our studies confirm that the presence of oxygen vacancies in the anatase TiO_2 assists the formation of the extra alloy layer (Ti_2AlO_4) by means of interface ionic relaxation. The identification of the alloy layer at the very initial stage of anatase TiO_2 growth confined in a single-layer-thick region at the film/substrate interface further confirms the truly 2D nature of the 2DEG in anatase TiO_2. Furthermore, our study also demonstrates that the quality of the anatase TiO_2 film depends on oxygen stoichiometry, which can be controlled to tune the functional properties and the emergent behavior of the heterointerface.

References

1. Ohtomo, A.; Hwang, H.Y. A high-mobility electron gas at the LaAlO$_3$/SrTiO$_3$ heterointerface. *Nature* **2004**, *427*, 423–427. [CrossRef] [PubMed]
2. Savoia, A.; Paparo, D.; Perna, P.; Ristic, Z.; Salluzzo, M.; Granozio, F.M.; Scotti di Uccio, U.; Richter, C.; Thiel, S.; Mannhart, J.; et al. Polar catastrophe and electronic reconstructions at the LaAlO$_3$/SrTiO$_3$ interface: Evidence from optical second-harmonic generation. *Phys. Rev. B* **2009**, *80*, 075110. [CrossRef]
3. Brinkman, A.; Huijben, M.; Van Zalk, M.; Zeitler, U.; Maan, J.C.; van der Wiel, W.; Rijnders, G.; Blank, D.H.A.; Hilgenkamp, H. Magnetic effects at the interface between non-magnetic oxides. *Nat. Mater.* **2007**, *6*, 493–496. [CrossRef] [PubMed]
4. Bi, F.; Huang, M.; Ryu, S.; Lee, H.; Bark, C.W.; Eom, C.B.; Irvin, P.; Levy, J. Room-temperature electronically-controlled ferromagnetism at the LaAlO$_3$/SrTiO$_3$ interface. *Nat. Commun.* **2014**, *5*, 5019. [CrossRef] [PubMed]
5. Adamo, C.; Perroni, C.A.; Cataudella, V.; De Filippis, G.; Orgiani, P.; Maritato, L. Tuning the metal-insulator transitions of (SrMnO$_3$)$_n$/(LaMnO$_3$)$_{2n}$ superlattices: Role of interfaces. *Phys. Rev. B* **2009**, *79*, 045125. [CrossRef]
6. Coll, M.; Fontcuberta, J.; Althammer, M.; Bibes, M.; Boschker, H.; Calleja, A.; Cheng, G.; Cuoco, M.; Dittmann, R.; Dkhil, B.; et al. Towards Oxide Electronics: A Roadmap. *Appl. Surf. Sci.* **2019**, *482*, 1–93. [CrossRef]
7. Thiel, S.; Hammerl, G.; Schmehl, A.; Schneider, C.W.; Mannhart, J. Tunable Quasi-Two-Dimensional Electron Gases in Oxide Heterostructures. *Science* **2006**, *313*, 1942–1945. [CrossRef]
8. Reinle-Schmitt, M.; Cancellieri, C.; Li, D.; Fontaine, D.; Medarde, M.; Pomjakushina, E.; Schneider, C.; Gariglio, S.; Ghosez, P.; Triscone, J.-M.; et al. Tunable conductivity threshold at polar oxide interfaces. *Nat. Commun.* **2012**, *3*, 932. [CrossRef]
9. Kalabukhov, A.; Gunnarsson, R.; Börjesson, J.; Olsson, E.; Claeson, T.; Winkler, D. Effect of oxygen vacancies in the SrTiO$_3$ substrate on the electrical properties of the LaAlO$_3$/SrTiO$_3$ interface. *Phys. Rev. B.* **2007**, *75*, 121404. [CrossRef]
10. Slooten, E.; Zhong, Z.; Molegraaf, H.J.A.; Eerkes, P.D.; De Jong, S.; Massee, F.; van Heumen, E.; Kruize, M.K.; Wenderich, S.; Kleibeuker, J.E.; et al. Hard X-ray photoemission and density functional theory study of the internal electric field in SrTiO$_3$/LaAlO$_3$ oxide heterostructures. *Phys. Rev. B* **2013**, *87*, 085128. [CrossRef]
11. Liu, Z.Q.; Li, C.J.; Lü, W.M.; Huang, X.H.; Huang, Z.; Zeng, S.W.; Qiu, X.P.; Huang, L.S.; Annadi, A.; Chen, J.S.; et al. Origin of the Two-Dimensional Electron Gas at LaAlO$_3$/SrTiO$_3$ Interfaces: The Role of Oxygen Vacancies and Electronic Reconstruction. *Phys. Rev. X* **2013**, *3*, 021010.
12. Moser, S.; Moreschini, L.; Jaćimović, J.; Barišić, O.S.; Berger, H.; Magrez, A.; Chang, Y.J.; Kim, K.S.; Bostwick, A.; Rotenberg, E.; et al. Tunable polaronic conduction in anatase TiO$_2$. *Phys. Rev. Lett.* **2013**, *110*, 196403. [CrossRef] [PubMed]
13. Rödel, T.C.; Fortuna, F.; Bertran, F.; Gabay, M.; Rozenberg, M.J.; Santander-Syro, A.F.; Le Fèvre, P. Engineering two-dimensional electron gases at the (001) and (101) surfaces of TiO$_2$ anatase using light. *Phys. Rev. B* **2015**, *92*, 041106. [CrossRef]
14. Wang, Z.; Zhong, Z.; Walker, S.M.; Ristic, Z.; Ma, J.; Bruno, F.Y.; Riccò, S.; SanGiovanni, G.; Eres, G.; Plumb, N.C.; et al. Atomically Precise Lateral Modulation of a Two-Dimensional Electron Liquid in Anatase TiO$_2$ Thin Films. *Nano Lett.* **2017**, *17*, 2561–2567. [CrossRef]
15. Ma, X.; Cheng, Z.; Tian, M.; Liu, X.; Cui, X.; Huang, Y.; Tan, S.; Yang, J.; Wang, B. Formation of Plasmonic Polarons in Highly Electron-Doped Anatase TiO$_2$. *Nano Lett.* **2020**, *21*, 430–436. [CrossRef]
16. Troglia, G.P.A.; Bigi, C.; Vobornik, I.; Fujii, J.; Knez, D.; Ciancio, R.; Drazic, G.; Fuchs, M.; Di Sante, D.; Sangiovanni, G.; et al. Evidence of a two-dimensional electron gas in a single-unit-cell of anatase TiO$_2$ (001). *Adv. Sci.* **2021**; *in press*.
17. Knez, D.; Dražić, G.; Chaluvadi, S.K.; Orgiani, P.; Fabris, S.; Panaccione, G.; Rossi, G.; Ciancio, R. Unveiling Oxygen Vacancy Superstructures in Reduced Anatase Thin Films. *Nano Lett.* **2020**, *20*, 6444–6451. [CrossRef]
18. Rossi, G.; Ciancio, R.; Africh, C.; Gotter, R.; Panaccione, G.; Ferranti, R. NFFA, Nanoscience Foundries & Fine Analysis (NFFA)—Trieste. *IRIS* **2011**, *16*, 8–12.
19. Chaluvadi, S.K.; Mondal, D.; Bigi, C.; Knez, D.; Rajak, P.; Ciancio, R.; Fujii, J.; Panaccione, G.; Vobornik, I.; Rossi, G.; et al. Pulsed laser deposition of oxide and metallic thin films by means of Nd:YAG laser source operating at its 1st harmonics: Recent approaches and advances. *J. Phys. Mater.* **2021**, *4*, 032001. [CrossRef]
20. Panaccione, G.; Vobornik, I.; Fujii, J.; Krizmancic, D.; Annese, E.; Giovanelli, L.; Maccherozzi, F.; Salvador, F.; De Luisa, A.; Benedetti, D.; et al. Advanced photoelectric effect experiment beamline at Elettra: A surface science laboratory coupled with Synchrotron Radiation. *Rev. Sci. Instrum.* **2009**, *80*, 043105. [CrossRef]
21. Bigi, C.; Tang, Z.; Pierantozzi, G.M.; Orgiani, P.; Das, P.P.K.; Fujii, J.; Vobornik, I.; Pincelli, T.; Troglia, A.; Lee, T.L.; et al. Distinct behavior of localized and delocalized carriers in anatase TiO$_2$ (001) during reaction with O$_2$. *Phys. Rev. Mater.* **2020**, *4*, 025801. [CrossRef]
22. Gobaut, B.; Orgiani, P.; Sambri, A.; Di Gennaro, E.; Aruta, C.; Borgatti, F.; Lollobrigida, V.; Céolin, D.; Rueff, J.-P.; Ciancio, R.; et al. Role of Oxygen Deposition Pressure in the Formation of Ti Defect States in TiO2(001) Anatase Thin Films. *ACS Appl. Mater. Interfaces* **2017**, *9*, 23099–23106. [CrossRef] [PubMed]
23. Orgiani, P.; Perucchi, A.; Knez, D.; Ciancio, R.; Bigi, C.; Chaluvadi, S.K.; Fujii, J.; Vobornik, I.; Panaccione, G.; Rossi, G.; et al. Tuning the Optical Absorption of Anatase Thin Films across the Visible-To-Near-Infrared Spectral Region. *Phys. Rev. Appl.* **2020**, *13*, 044011. [CrossRef]
24. Giannozzi, P.; Baroni, S.; Bonini, N.; Calandra, M.; Car, R.; Cavazzoni, C.; Ceresoli, D.; Chiarotti, G.L.; Cococcioni, M.; Dabo, I.; et al. QUANTUM ESPRESSO: A modular and open-source software project for quantum simulations of materials. *J. Phys. Condens. Matter Inst. Phys. J.* **2009**, *21*, 395502. [CrossRef] [PubMed]

25. Haas, P.; Tran, F.; Blaha, P. Calculation of the lattice constant of solids with semilocal functionals. *Phys. Rev. B* **2009**, *79*, 085104. [CrossRef]

26. Koch, C.T. Determination of Core Structure Periodicity and Point Defect Density along Dislocations. Ph.D. Thesis, Arizona State University, Phoenix, AZ, USA, 2002.

27. Ciancio, R.; Carlino, E.; Aruta, C.; Maccariello, D.; Granozio, F.M.; di Uccio, U.S. Nanostructure of buried interface layers in TiO2anatase thin films grown on LaAlO$_3$ and SrTiO$_3$ substrates. *Nanoscale* **2011**, *4*, 91–94. [CrossRef]

28. Ciancio, R.; Carlino, E.; Rossi, G.; Aruta, C.; Di Uccio, U.S.; Vittadini, A.; Selloni, A. Magnéli-like phases in epitaxial anatase TiO$_2$ thin films. *Phys. Rev. B* **2012**, *86*, 104110. [CrossRef]

29. Howie, A. Image Contrast and Localized Signal Selection Techniques. *J. Microsc.* **1979**, *117*, 11–23. [CrossRef]

30. Kirkland, E.J.; Loane, R.F.; Silcox, J. Simulation of annular dark field stem images using a modified multislice method. *Ultramicroscopy* **1987**, *23*, 77–96. [CrossRef]

31. Kirkland, E.J. *Advanced Computing in Electron Microscopy*; Plenum Press: New York, NY, USA, 1998.

32. Wang, Z.; Zeng, W.; Gu, L.; Saito, M.; Tsukimoto, S.; Ikuhara, Y. Atomic-scale structure and electronic property of the LaAlO$_3$/TiO$_2$ interface Atomic-scale structure and electronic property of the LaAlO$_3$/TiO$_2$ interface. *J. Appl. Phys.* **2014**, *108*, 113701–113709. [CrossRef]

33. Zheng, S.; Fisher, C.A.J.; Kato, T.; Nagao, Y.; Ohta, H.; Ikuhara, Y. Domain formation in anatase TiO$_2$ thin films on LaAlO$_3$ substrates. *Appl. Phys. Lett.* **2012**, *101*, 191602. [CrossRef]

34. Jain, A.; Ong, S.P.; Hautier, G.; Chen, W.; Richards, W.D.; Dacek, S.; Cholia, S.; Gunter, D.; Skinner, D.; Ceder, G.; et al. Commentary: The Materials Project: A materials genome approach to accelerating materials innovation. *APL Mater.* **2013**, *1*, 011002. [CrossRef]